HHS Public Access

Author manuscript

Neuron. Author manuscript; available in PMC 2019 February 07.

Published in final edited form as:

Neuron. 2018 February 07; 97(3): 586–595.e4. doi:10.1016/j.neuron.2018.01.013.

Thermal excitation of the mechanotransduction apparatus of hair cells

Julien B. Azimzadeh, **Brian A. Fabella**, **Nathaniel R. Kastan**, and **A. J. Hudspeth**[*]

Howard Hughes Medical Institute and Laboratory of Sensory Neuroscience, The Rockefeller University, 1230 York Avenue, New York, NY 10065, USA

SUMMARY

Although a hair bundle is normally deflected by mechanical stimuli, we found that irradiation of a hair cell from the bullfrog's sacculus with ultraviolet light causes rapid motion of the hair bundle toward its tall edge. This movement is associated with opening of mechanotransduction channels and disappears when tip links are disrupted. We localized the absorptive element responsible for the motion to the region directly below the hair bundle and measured an action spectrum similar to the absorption spectra of mitochondrial constituents. Temperature measurements revealed heating around the site of absorption; direct heating of the hair bundle confirmed that the response to light is mediated through heat. Although mechanical offsets of the hair bundle revealed that heat softens gating springs, it also acts directly to open transduction channels. This study identifies an unconventional method of hair-cell stimulation and clarifies the previously unexplained sensitivity of auditory organs to thermal stimulation.

eTOC BLURB

Azimzadeh *et al*. show that hair cells of the inner ear can be stimulated by light without external or genetic manipulation. Chromophores in mitochondria convert light to heat, which subsequently acts on elements of the hair bundle to stimulate it.

INTRODUCTION

A hair cell of the auditory, vestibular, or lateral-line system transduces mechanical energy into electrical signals by means of its hair bundle. Each bundle is an upright cluster of actin-filled protuberances called stereocilia, which increase in length from one edge of the hair cell to that opposite to produce a staircase (Figure 1A). Along the same axis, each shorter stereocilium is attached to its tallest neighbor by a cadherin-based strand, the tip link.

[*]Lead Contact: hudspaj@rockefeller.edu.

AUTHORS' CONTRIBUTIONS

J.B.A. and A.J.H. designed the experiments; B.A.F. wrote the software; B.A.F. and J.B.A. prepared the specialized apparatus; J.B.A. and N.R.K. conducted the experiments; J.B.A. and A.J.H. wrote the paper and prepared the figures.

DECLARATION OF INTERESTS

The authors declare no competing interests.

Moving the hair bundle in the positive direction, toward its tall edge, increases the tension in each tip link, which in turn opens mechanically sensitive ion channels at the link's lower insertion. The ensuing influx of cations initiates an electrical response that propagates by means of a chemical synapse to an afferent nerve fiber. A myosin-based motor at the upper end of each link ascends or descends a stereocilium to maintain the tip-link tension within a narrow range, thus effecting adaptation that restores the hair bundle's mechanical sensitivity during protracted stimulation.

Hair cells are not only passive detectors but also active amplifiers (Ashmore, 1987; Brownell et al., 1985; Hudspeth, 2014; Martin and Hudspeth, 1999). Their capacity to amplify sound stems from a combination of somatic motility and active hair-bundle motility, the ability of a bundle to produce force that augments a mechanical stimulus. One mechanism by which the hair bundle might supplement the energy in a stimulus is fast adaptation, the rapid reclosure of mechanotransduction channels after stimulation (Benser et al., 1996; Howard and Hudspeth, 1987). The concerted closure of channels produces a rapid mechanical twitch that augments mechanical stimuli (Benser et al., 1996; Choe et al., 1998; Hudspeth, 2008; Kennedy et al., 2005). Although its mechanism in mammals remains a subject of debate (Bozovic and Hudspeth, 2003; Cheung and Corey, 2006; Corns et al., 2014; Howard and Hudspeth, 1988; Howard and Spudich, 1996; Peng et al., 2013; Tinevez et al., 2007; Wu et al., 1999), fast adaptation is believed to arise from the direct activity of Ca^{2+} on the transduction channel, an associated relaxation element, or the motors responsible for slow adaptation.

The initial aim of this study was to elucidate the role of Ca^{2+} in fast adaptation by generating intracellular surges in Ca^{2+} concentration without altering the state of the mechanotransduction channels or the associated components. We used a light-sensitive, Ca^{2+}-loaded cage compound to release Ca^{2+} in hair cells by ultraviolet (UV) irradiation (Ellis-Davies and Kaplan, 1994). To our surprise, irradiation in either the presence or the absence of the caged Ca^{2+} compound caused rapid motion of hair bundles. Because this unexpected sensitivity to light provides insight into the transduction process and might be useful in stimulating hair cells, we undertook a detailed analysis of its mechanism.

RESULTS

Light-evoked hair-bundle motion

We studied the responses of hair bundles from the bullfrog's sacculus to pulses of ultraviolet irradiation at a wavelength of 375 nm. When placed within or directly adjacent to a 6 μm × 12 μm oval beam of ultraviolet light, a hair bundle moved rapidly towards its kinocilium for the duration of the light pulse and relaxed to its original position upon light offset (Figure 1B). In healthy preparations, this phenomenon was observed in over 90 % of irradiated hair cells. Light-evoked motion was always directed towards the kinocilium, regardless of a bundle's orientation within the epithelium (Movie S1). When we irradiated a hair bundle from a direction orthogonal to its plane of symmetry, hair-bundle motion was no different from that elicited by apical irradiation, indicating that photonic pressure did not underlie the movement (Figure S1A).

The timecourse of light-evoked hair-bundle displacement varied among bundles: whereas some bundles exhibited a slow, asymptotic displacement, others displayed rapid and biphasic motion (Figure 1B). The amplitude of light-evoked motion varied as well, ranging from negligible to 300 nm. However, all hair bundles exhibited a linear power-displacement relation at low power densities (Figure 1C). There was no apparent threshold for the movements; instead, a bundle's displacement response fell into the noise floor as the irradiation decreased.

The structure and transduction mechanism of the hair bundle are highly conserved throughout the vertebrates. Although we conducted most of our experiments on hair cells of the bullfrog's sacculus owing to the large size and robustness of their hair bundles, we also tested hair cells from the murine utricle as representatives of mammalian hair cells. Irradiation with ultraviolet light produced hair-bundle motions similar to those observed for frog bundles (Figure S1B).

As depicted in a video capturing both a cell's soma and its hair bundle, light-evoked motion was confined to the bundle (Movie S2). This observation was confirmed by visualizing the light-evoked motion after image subtraction (Figure S1C). Because movement was confined to the hair bundle and restricted to the bundle's direction of mechanical sensitivity, we suspected that the mechanoelectrical-transduction apparatus was involved in the response. To test this, we examined a hair bundle's response before and after the iontophoretic disruption of tip links by the application of ethylene glycol-bis (β-aminoethyl ether)-*N,N,N′,N′*-tetraacetic acid (EGTA). After tip-link rupture, a hair bundle no longer moved in response to ultraviolet irradiation, indicating that the mechanotransduction apparatus was required for the response (Figure 1D). To determine whether kinocilia were involved in light-evoked motion, we irradiated three hair bundles before and after microdissection of their kinocilia. We observed no significant changes in the bundles' responses to ultraviolet illumination (Figure S2).

We next sought to determine whether ultraviolet irradiation opens mechanotransduction channels. Microelectrode recordings revealed that each of 31 hair cells with intact tip links depolarized in response to irradiation, whereas all 18 cells with EGTA-disrupted links did not (Figure 2A). To confirm that depolarization originated from the mechanotransduction current, we performed tight-seal, whole-cell recordings from 12 hair cells. Irradiation elicited an inward current that was interrupted by gentamicin, a blocker of mechanotransduction channels (Figure 2B,C). The average maximal current evoked by irradiation of 12 cells was 68 pA, as compared to typical values of 150 pA evoked by mechanical stimulation (Assad et al., 1989). As it does with mechanical stimulation, the mechanotransduction current adapted in response to light stimulation (Figure S3). These results confirmed that mechanotransduction channels were the source of the light-evoked electrical activation of hair cells.

Gating springs slacken upon the opening of mechanotransduction channels, resulting in a positive movement of the hair bundle (Howard and Hudspeth, 1988), so the bundle motion evoked by illumination might result from channel gating. To examine this possibility, we simultaneously recorded a hair cell's membrane potential and its hair bundle's position

while iontophoretically releasing gentamicin to block channel gating. Although the light-evoked receptor potential vanished during a large release of gentamicin, indicating complete blockage of mechanotransduction channels, the corresponding hair-bundle displacement did not decline to zero (Figure 2D,E). The gating of mechanotransduction channels evidently underlay slightly more than half of the light-evoked motion of the hair bundle, with the balance contributed by another process. The displacement evoked by this second process might be enhanced by gentamicin treatment, resulting in a decrement in the decay of hair-bundle displacement relative to the decay of the voltage response. Such a mismatch appears in our data, for the receptor potential decays to zero with 5 nA of iontophoretic current, whereas the displacement is only mildly reduced at that level. We interpret this effect in more detail in the Discussion.

Intracellular chromophores

To identify the molecular underpinnings of light-evoked motion, we sought to localize the cellular components responsible for the conversion of light into hair-bundle motion. We confined ultraviolet irradiation to subcellular regions with a custom-built patterned-illumination system based on a digital micromirror device (Figure 3A). We then positioned an isolated hair cell with its plane of symmetry orthogonal to the beam of light and irradiated distinct areas of the cell while measuring the displacement of its hair bundle. To our surprise, a cell responded maximally to light directed at the apex of its soma but just below its hair bundle (Figure 3B,C). Furthermore, the response was minimal when irradiation was confined to the hair bundle. Results from five cells show that irradiation of the cuticular plate produced 70 ± 22 % of the motion elicited by total irradiation, whereas irradiation of the hair bundle yielded only 24 ± 14 %. The absorbers responsible for hair-bundle motion therefore lay at the hair bundle's base.

To characterize the molecular absorbers underlying the photostimulation of hair cells, we obtained a coarse action spectrum of hair-bundle displacement. We recorded the motion of bundles in response to light in six different wavelength ranges, each encompassing the same stimulus power. The resulting action spectrum revealed that illumination was most efficient near a wavelength of 400 nm (Figure 3D). This sensitivity resembles the absorption spectra of nicotinamide adenine dinucleotide (NADH), flavoproteins, and hemoproteins, the principal intracellular absorbers of ultraviolet light (Bin Liu et al., 2010; Butt and Keilin, 1962; Siegel et al., 1959). Because these molecules fluoresce, we were able to localize them in hair cells through fluorescence microscopy. The chromophores were found to occur primarily near the cuticular plate and the base of a cell, but were absent from the hair bundle (Figure 3E). The two regions of strong fluorescence were dense with mitochondria and lesser numbers of peroxisomes, organelles filled with NADH, flavins, and cytochromes (Figure 3F). These organelles are required to satisfy the heavy metabolic demands of the hair bundle and synaptic machinery. Hair-bundle motion thus appeared to be linked to light absorption by intracellular chromophores in mitochondria and peroxisomes.

Thermal pulses

A portion of the energy delivered to intracellular chromophores by ultraviolet light might be released as heat. By measuring the temperature with the calibrated resistance of a glass

micropipette (Yao et al., 2009a), we sought to quantitate this effect and determine whether it underlay light-evoked hair-bundle motion (Figure S4). As expected from water's low absorption of ultraviolet light, irradiation of saline solution did not generate a measurable temperature increase. Irradiation of 25 hair cells, however, resulted in detectable local increases in temperature (Figure 4A). The action spectrum of this effect matched that of the hair bundle's displacement, suggesting that the same molecular source mediated both bundle motion and heat production (Figure 4B).

Measurements of the light-evoked temperature changes along the sides of three dissociated hair cells revealed that the locale of maximal heat production was near the cellular apex, adjacent to the cuticular plate (Figure 4C). Furthermore, the temperature gradient above a hair cell irradiated in the sensory epithelium matched a model of heat diffusion from mitochondrial sources (Figure 5). If heat arises from the irradiation of intracellular absorbers, we might expect other cell types to experience temperature changes as well. Indeed, ultraviolet illumination of red blood cells and saccular supporting cells also resulted in local temperature increases (Fig. S5A). Although the temperature increase produced by irradiation varied between cell types, the action spectrum of the effect was similar among all cells, supporting the conclusion that the absorbers responsible for heating were ubiquitous (Figure S5B).

To determine whether the temperature increase elicited by ultraviolet irradiation caused hair-bundle motion, we recorded the response of a hair cell to temperature pulses generated by infrared heating of water. A hair cell was placed in the paths both of an ultraviolet beam traversing the objective lens and of an infrared beam emanating from a 100 μm-diameter optical fiber positioned about 100 μm from the hair bundle (Figure 4D). In response to either ultraviolet or infrared irradiation, we simultaneously recorded hair-bundle motion and the temperature at a distance of 2 μm from the hair bundle. With the infrared power adjusted to generate a temperature increase at the hair bundle similar to that caused by the ultraviolet pulse, we observed nearly identical hair-bundle displacements for both wavelengths (Figure 4E).

We confirmed that heating effects hair-bundle motion by exchanging a saline solution based on ordinary water (H_2O), the primary absorber of infrared light in our system, with a solution containing deuterium oxide (D_2O). Because the absorption coefficient (Bayly et al., 1963) of D_2O at 1470 nm is only 0.5 % that of H_2O, more infrared radiation reached an irradiated hair bundle in D_2O-based saline solution; nevertheless, a smaller temperature increase ensued. For three hair cells in D_2O-based saline solution, we measured a reduction of 63 % in hair-bundle displacement and a corresponding 60 % decrease in the infrared light-evoked temperature increase (Figure 4E). The residual temperature increase in D_2O likely stems from the heating of intracellular H_2O that was not replaced by the exchange of the extracellular solution. For ultraviolet light, which traverses H_2O and D_2O about equally well, neither the displacement response nor the temperature increase was altered by the exchange of liquids. This observation confirms that heat and not light was the primary effector of hair bundle motion and that the relevant site of ultraviolet absorption was intracellular.

To further illustrate that a local pulse of heat could evoke hair-bundle motion, we situated the tip of a 5 μm-diameter carbon fiber next to a dissociated hair cell. When the fiber's shaft was heated by illumination with ultraviolet light, the direct thermal stimulus produced hair-bundle motion that disappeared upon retraction of the fiber (Figure 6).

Effects of heat

Heat pulses exert a variety of effects on excitable biological tissue. Because the heat-evoked stimulation of hair cells required intact tip links, it was unlikely to have been mediated by thermally gated channels, changes in membrane capacitance, or other processes independent of the hair bundle. We therefore investigated whether heat pulses stimulated hair bundles by mechanically altering components of the transduction apparatus.

The position of a hair bundle is determined by the forces in two sets of opposing elastic elements, gating springs and stereociliary pivots. Given this arrangement, positively directed motion might ensue either from loosening the gating springs or from stiffening the stereociliary pivots. These alternatives could be differentiated with the help of offset displacements provided by a mechanical-stimulus fiber. If a decrease in tip-link stiffness were to underlie heat-mediated hair-bundle motion, positive offsets would increase the amplitude of motion evoked by the stiffness change, whereas negative offsets would reduce it (Figure 7A). The opposite result would be expected if the thermal motion were to result from an increase in the stiffness of the stereociliary pivots.

To determine which elastic element underlay heat-mediated hair-bundle motion, we irradiated ten hair cells whose bundles had been offset by either a flexible glass fiber or a fluid jet. Because the amplitude of light-evoked motion consistently increased with positive offsets (Figure 7B), heat apparently softened the gating springs, which probably include the tip links and other components in series with them, such as the insertional plaques and adaptation motors. To verify that heat did not alter the stiffness of the stereociliary pivots, we severed the tip links and measured the stiffness of stereociliary pivots before and during irradiation (Figure S6). No significant change in stiffness was detected in any of four experiments.

If a hair bundle were prevented from moving towards its tall edge, relaxation of the gating springs should close the mechanotransduction channels that are open at rest. In support of this hypothesis, when the motion of five hair bundles was arrested by a stiff glass fiber, their light-evoked responses changed from depolarization to hyperpolarization (Figure 7C,D).

DISCUSSION

The responses presented in this study reflect an unexpected mechanism of hair-cell stimulation by light-evoked heat pulses. During illumination by ultraviolet light, heat is generated by the excitation of intracellular chromophores, the preponderance of which reside in mitochondria (Berns et al., 1970; Salet, 1972). The thermal pulses alter the mechanical properties of the hair bundle, simultaneously opening the transduction channels and displacing the bundle towards its tall edge. This response mechanism relies on the softening of gating springs, and is thus specific to hair cells. The transformation of light into thermal

energy, however, is a ubiquitous property of cells that depends on their concentration of chromophores. Hair cells may be particularly prone to photothermal stimulation owing to their high concentration of mitochondria. We nonetheless anticipate that other mitochondrion-rich cells, such as myocytes, hepatocytes, and neurons, can respond to irradiation-evoked heating, especially if the cells contain highly temperature-sensitive molecules. Heterogeneity in the density and distribution of mitochondrial absorbers from one hair cell to another likely accounts for much of the variability that we observed in the amplitude and timecourse of responses.

The ability of a hair cell to respond to thermal pulses hinges upon the high sensitivity of its mechanical antenna, the hair bundle. A bundle's transduction channels lie in parallel, an arrangement that divides tension equally among the gating springs (Kozlov et al., 2007). When a fraction of these springs relax, the tension is redistributed among the remainder, increasing the open probability of the associated channels. These open channels represent only a fraction of a bundle's total, as supported by our observation that the maximal current evoked by irradiation is only 45 % of that evoked mechanically. The relaxation of gating springs themselves is enough to generate hair-bundle motion. The contribution of gating springs to thermally induced motion can be increased by treatments that raise the baseline tip-link tension, such as the blockage of mechanotransduction pores with gentamicin. The reduction of Ca^{2+} influx when pores are blocked enhances the activity of myosin motors and increases the tip-link tension. The overall hair-bundle displacement accordingly decays less with gentamicin treatment than does the hair cell's voltage response (Figure 2D).

Although heat appears to relax the gating springs, the present results are not readily explicable on the basis of that effect alone. Prolonged relaxation of the gating springs should cause a net decrease in channel opening in the steady state. It is thus likely that thermal pulses alter an additional property of the hair bundle. One possibility is that heating both softens the gating springs and promotes channel opening, so that the thermal responses reflect partly antagonistic influences. The amount of heating in these experiments is by itself insufficient to open channels, for severing the tip links abolishes thermal responsiveness. When a hair bundle is held at its resting position by an external fiber, the closure of channels during illumination implies that the relaxation of gating springs outweighs the propensity for channel opening.

The present experiments provide no evidence about the basis of gating-spring relaxation in response to heating. The tip links might grow more compliant, for example by the release of stabilizing Ca^{2+} ions from protocadherin 15 and cadherin 23 or by partial unfolding of extracellular cadherin domains. Fewer myosin molecules might bind at the insertional plaques atop tip links, thus reducing the stiffness of the assembly (Berger and Hudspeth, 2017). The relaxation elements hypothesized to explain fast adaptation might display thermal softening (Bozovic and Hudspeth, 2003). Finally, the actin cores of stereocilia might shrink owing to the negative thermal expansion coefficient of filamentous actin (Rosin et al., 2014). As a result of the systematic differences in length between adjacent stereocilia, thermal contraction of actin could relax gating springs.

It is also unclear how a temperature step would alter the open probability P_o of the transduction channels. For a channel considered in isolation, this probability is a function of the difference ΔG in Gibbs free energy between the channel's open and closed states:

$$P_o = \frac{1}{1+e^{\Delta G/kT}} = \frac{1}{1+e^{\Delta H/kT}e^{-\Delta S/k}},$$

in which ΔH and ΔS are respectively the enthalpic and entropic components, k is the Boltzmann constant, and T is the absolute temperature. In the simplest analysis, the temperature dependence of the open probability may be found by differentiating P_o with respect to T:

$$\frac{dP_o}{dT} = \frac{-1}{\left(1+e^{\Delta H/kT}e^{-\Delta S/k}\right)^2}\left(e^{\Delta H/kT}e^{-\Delta S/k}\right)\left(\frac{-\Delta H}{kT^2}\right) = P_o(1-P_o)\left(\frac{\Delta H}{kT^2}\right).$$

For a resting open probability of 0.2, the free energy of an open channel exceeds that of a closed one (Corey, 1980) by about 1 kT. If this value were entirely enthalpic, the thermal sensitivity of the open probability at room temperature would be only 0.0007 K^{-1}. A temperature increase of 10 °C, near the largest observed in this study, would raise the open probability by less than 0.01, a value well below that needed to explain our results.

The calculation above does not take into account the intrinsic energy difference between the closed and open states of a channel when it is disconnected from its tip link. This value, $\Delta G^{\emptyset}$, is estimated at 10 kT per molecule (Hudspeth, 1992). Even if this change were entirely enthalpic, the change in open probability would remain less than 0.1 for a 10 °C temperature change. Only if the opening transition were to involve a substantial increase in entropy might the difference in intrinsic enthalpy exceed that in free energy. Unfortunately, though, there are no measurements bearing on this issue.

Light-based stimulation of the peripheral auditory system is of clinical interest owing to its potential use in cochlear prostheses (Hernandez et al., 2014; Richardson et al., 2017; Richter et al., 2013). Although infrared light has been used to stimulate a variety of peripheral nerves, the power density required to activate the auditory and vestibular nerves is only a fraction of that required for others (Goyal et al., 2012; Wells et al., 2005). This distinction likely reflects the generation during optical stimulation of optoacoustic pulses that hair cells can detect (Kallweit et al., 2016; Teudt et al., 2011). That ablation of hair cells abolishes the auditory-nerve response to infrared pulses accords with this hypothesis, suggesting that most responses to optical stimulation have been mediated primarily by optoacoustic phenomena (Kallweit et al., 2016; Teudt et al., 2011; Thompson et al., 2015; Verma et al., 2014).

The present results, however, cannot be explained by optoacoustic stimulation. Optoacoustic waves are generated under conditions of thermal confinement, a regime in which heat is deposited in a region faster than it can be removed by diffusion (Paltauf et al., 1998). The longest irradiation pulse permitting thermal confinement is given by

$$\tau_{th} = \frac{\delta^2}{4\kappa},$$

in which δ is the beam's radius or the optical penetration depth of the irradiating light, whichever is smaller, and κ is the thermal diffusivity of water (Paltauf et al., 1998), $1.43 \cdot 10^{-7}$ $m^2 \cdot s^{-1}$. The primary absorber in mitochondria is cytochrome c, with a molar absorption coefficient (Butt and Keilin, 1962) of 0.06 $M^{-1} \cdot cm^{-1}$ at 405 nm. The absorption coefficient for cytochrome c at a concentration of 100 μM in mitochondria (Gupte and Hackenbrock, 1988) is $6 \cdot 10^{-6}$ cm^{-1}. For a mitochondrion-filled cylinder of diameter 10 μm and height 5 μm at the apex of a hair cell, δ is 5 μm. τ_{th} is therefore 43 μs, or only one-thousandth our typical pulse duration of 40 ms. Thermal confinement should not be possible and no optoacoustic wave should be generated. This analysis is supported by our observation that hair bundles do not respond to light after their tip links have been ruptured. If hair-bundle motion arose from optoacoustic stimulation, the response would persist after that treatment.

Two alternative mechanisms have been proposed for hair-cell stimulation by irradiation. In the first, light evokes a rapid heat pulse that alters the membrane's capacitance and depolarizes the cell (Rabbitt et al., 2016). The change in capacitance stems from asymmetric movement of ions present on the two sides of the plasma membrane, a general mechanism that does not require ion channels (Liu et al., 2014; Shapiro et al., 2012). The second proposition is that illumination releases Ca^{2+} from mitochondrial stores (Rajguru et al., 2011). Although light-induced Ca^{2+} release has not been observed in hair cells, it occurs in cardiomyocytes as well as vestibular- and spiral-ganglion neurons (Dittami et al., 2011; Lumbreras et al., 2014). Neither of these two mechanisms can explain the results presented in this study. If a change in cellular capacitance elicited the response to light, neither tip-link rupture nor transduction-channel blockage would eliminate the response. Similarly, if Ca^{2+} release from intracellular stores were responsible for hair-cell stimulation, the electrical response would persist after tip-link rupture. We observed instead that the thermal response requires the integrity of tip links and the patency of the transduction-channel pores.

Although we have focused on the effects of heating on mechanoelectrical transduction, we anticipate that illumination of the mitochondria elsewhere in hair cells also has effects. In particular, irradiation of the mitochondria clustered at the basal ends of these cells might cause heating and Ca^{2+} release in the region of the ribbon synapses. The resultant enhancement of transmitter release could make an additional contribution to the eighth-nerve responses to light.

The phenomenon described here, which permits stimulation of hair cells without genetic manipulation or mechanical contact, allows previously impossible studies. For example, irradiation might be used to study the activity of mammalian cochlear hair cells without the generation of a traveling wave. In addition, the ability to rapidly and synchronously stimulate groups of hair cells would facilitate studies of processes subsequent to the receptor potential, such as synaptic transmission. Finally, irradiation could be employed to verify that a hair cell's transduction apparatus is intact.

STAR METHODS

CONTACT FOR REAGENT AND RESOURCE SHARING

Requests for information and resources should be directed to the Lead Contact, Dr. A. J. Hudspeth (hudspaj@rockefeller.edu).

EXPERIMENTAL MODEL AND SUBJECT DETAILS

All procedures were approved by the Institutional Animal Care and Use Committee of The Rockefeller University. Sacculi were extracted from adult male and female bullfrogs (*Rana catesbeiana*) as described (Azimzadeh and Salvi, 2017). Dissections were performed in artificial perilymph containing 114 mM Na^+, 2 mM K^+, 2 mM Ca^{2+}, 118 mM Cl^-, 5 mM HEPES, and 3 mM **D**-glucose. The pH was 7.2–7.3 and the osmolarity was 230 mOsm·kg^{-1}. Once isolated from the inner ear, each saccular macula was digested in 67 mg·L^{-1} protease XXIV (P8038, Sigma) for 30 min at 22 °C before the otolithic membrane was carefully removed with a fine eyelash. The organ was secured in a recording chamber with pins, held to the bottom of the chamber with cyanoacrylate adhesive (VetBond, 3M), or mounted across a 1 mm-diameter hole in aluminum foil with the same adhesive.

Utriculi were obtained from 38-week-old C3H/HeNCrl mice (*Mus musculus*) of both sexes (Charles River, Wilmington, MA). Mice were anesthetized with isoflurane, euthanized by cervical dislocation, and decapitated. Under a dissecting microscope, each utriculus was extracted from the skull into ice-cold Hank's balanced salt solution (HBSS, ThermoFisher). The otic capsule was opened medially and the roof of the liberated utriculus was removed. Following a 20 min incubation in 100 mg·L^{-1} protease XXIV at room temperature, the utricular macula was mounted on a chamber and secured with pins. The otolith was gently removed with a fine eyelash, ensuring minimal contact with the sensory epithelium. Experiments on these preparations were performed in HBSS, which contains 1.26 mM Ca^{2+}.

METHOD DETAILS

Experimental preparation—All procedures were approved by the Institutional Animal Care and Use Committee of The Rockefeller University. Sacculi were extracted from adult male and female bullfrogs (*Rana catesbeiana*) as described (Azimzadeh and Salvi, 2017). Dissections were performed in artificial perilymph containing 114 mM Na^+, 2 mM K^+, 2 mM Ca^{2+}, 118 mM Cl^-, 5 mM HEPES, and 3 mM **D**-glucose. The pH was 7.2–7.3 and the osmolarity was 230 mOsm·kg^{-1}. Once isolated from the inner ear, each saccular macula was digested in 67 mg·L^{-1} protease XXIV (P8038, Sigma) for 30 min at 22 °C before the otolithic membrane was carefully removed with a fine eyelash. The organ was secured in a recording chamber with pins, held to the bottom of the chamber with cyanoacrylate adhesive (VetBond, 3M), or mounted across a 1 mm-diameter hole in aluminum foil with the same adhesive.

Utriculi were obtained from 38-week-old C3H/HeNCrl mice (*Mus musculus*) of both sexes (Charles River, Wilmington, MA). Mice were anesthetized with isoflurane, euthanized by cervical dislocation, and decapitated. Under a dissecting microscope, each utriculus was extracted from the skull into ice-cold Hank's balanced salt solution (HBSS, ThermoFisher).

The otic capsule was opened medially and the roof of the liberated utriculus was removed. Following a 20 min incubation in 100 $mg \cdot L^{-1}$ protease XXIV at room temperature, the utricular macula was mounted on a chamber and secured with pins. The otolith was gently removed with a fine eyelash, ensuring minimal contact with the sensory epithelium. Experiments on these preparations were performed in HBSS, which contains 1.26 mM Ca^{2+}.

Hair-cell isolation—Frog maculae destined for experiments on isolated hair cells were dissected in perilymph containing 100 μM free Ca^{2+}. After removal of the inner ear, the semicircular canals were trimmed to the base of their ampullae, which were sealed with cyanoacrylate adhesive expelled from a fine glass pipette. The pipette was fabricated by pulling a glass capillary to an external diameter of 100–200 μm. Before being filled with cyanoacrylate adhesive, the pipette's tip was transiently filled with lubricant (WD-40 Company). Adhesive was delivered to the trimmed ampullae by positive pressure.

After all the ampullae had been glued shut, the perilymphatic cistern was removed and the inner ear was placed for 12 min at 22 °C in Ca^{2+}-free solution consisting of 114 mM Na^+, 2 mM K^+, 1 mM EGTA, 1 mM Mg^{2+}, 120 mM Cl^-, 3 mM **D**-glucose, and 5 mM HEPES at pH 7.2. Following the return of the inner ear to 100 μM Ca^{2+} solution, the saccular macula was isolated and digested in 67 $mg \cdot L^{-1}$ protease XXIV (P8038, Sigma) for 30 min at room temperature.

For experiments with mechanically isolated hair cells, the saccular macula was held with pins in a chamber with a concanavalin A-coated slide at its bottom. Hair cells were gently flicked from the sensory epithelium with a fine eyelash and allowed to settle for 10 min.

When extruded hair cells were sought, the macula was secured in a chamber by two mounting pins, which applied a slight tension that encouraged hair cells to gradually extrude from the epithelium. Cellular extrusion commenced approximately 20 min after mounting and continued for several hours. The liberated hair cells could be used *in situ* or individually held in a polished glass pipette. The pipette was prepared by pulling a pair of fine borosilicate microelectrodes, one of which was used to scratch and cleave the other at a location where its inner diameter was 9 μm. The broken pipette was fire-polished smooth, filled with saline solution, and mounted in an electrode holder. Hair cells were picked up and held by pipettes under gentle negative pressure.

Folded-epithelium preparation—The saccular macula was dissected and digested as above. By careful probing with the tip of a fine eyelash, the saccular epithelium was separated from the underlying connective tissue and folded along its plane of mirror symmetry. A gold electron-microscopy grid (G100-Au, Electron Microscopy Sciences) was rested upon the folded epithelium to stabilize it and maintain the crease (Kozlov et al., 2007). Hair cells were visualized from a direction orthogonal to their axes of sensitivity.

Microscopic apparatus—Hair cells were visualized with differential-interference-contrast optics at 60X magnification on an upright microscope (BX51WI, Olympus). For recordings of hair-bundle displacement, preparations were illuminated with a 630 nm light-emitting diode (UHP-LED-630, Prizmatix). Images and video were acquired with a charge-

coupled device (CCD) camera (OLY-150, Olympus). High-frame-rate videos were acquired with a high-speed CCD camera (MotionScope 2000S, Redlake).

Photometric recording—When the sample was illuminated as described above, light piping through stereocilia resulted in a high-contrast image of a hair bundle's tip that was imaged on the photodiode at a magnification of 1250X. Output from the photodiode was low-pass filtered at 4 kHz with a Bessel filter (BenchMaster 8, Kemo). The photodiode signal was calibrated by translating a bundle's image in 10 μm steps with a mirror mounted on a piezoelectric actuator (PA 120/14 SG, Piezosystem Jena). This actuator was driven by a 300 mA amplifier and calibrated by a heterodyne interferometer (ENV 300SG, Piezosystem Jena; OFV 501, Polytec).

Electrophysiology—Hair-cell currents were recorded with tight-seal, whole-cell electrodes filled with potassium gluconate internal solution containing 117 mM K^+, 2 mM Na^+, 4 mM Mg^{2+}, 117 mM gluconate, 1 mM ATP, 2 mM Cl^-, 5 mM EGTA, and 5 mM HEPES at pH 7.2–7.3. Electrodes were pulled to a tip resistance of 3–8 MΩ with an electrode puller (P-2000, Sutter Instruments) and were coated with nail polish to decrease the transmural capacitance. Hair cells were held at −70 mV with a voltage-clamp amplifier (Axopatch 200B, Molecular Devices) without compensation for the diffusional tip potential.

Sharp microelectrodes were pulled with an electrode puller (P-80/PC, Sutter) and their tips were bent through an angle of 60° to allow vertical insertion into the hair-cell apex (Hudspeth and Corey, 1978). When filled with 3 M KCl, tip resistances were 100–300 MΩ. Intracellular voltage was recorded by a DC-coupled amplifier (Axoclamp 2B, Axon Instruments) set to pass 0–3 kHz.

We used iontophoresis to release EGTA and gentamicin onto hair bundles. An iontophoretic electrode was fabricated from a glass capillary pulled with an electrode puller (P-80/PC, Sutter Instruments) and filled with 500 mM EGTA in 1 M NaOH or with 500 mM gentamicin sulfate. The electrode's tip was placed approximately 3 μm from the top of a hair bundle. An amplifier was used to pass currents of up to ±100 nA through the electrode to elicit release of its contents (Axoclamp 2B; Axon Instruments). A holding current was used between current pulses to prevent leakage of the electrode's contents onto the hair bundle.

Mechanical stimulation—Mechanical stimuli were delivered by flexible or stiff glass fibers fabricated from borosilicate capillaries (1B120F-3, World Precision Instruments). A flexible probe was made by first thinning a capillary with an electrode puller (P-2000, Sutter Instruments) and subsequently pulling its tip laterally with a 120 V solenoid to form a 90° angle with the capillary shaft. Each probe was 0.5–0.8 μm in diameter and no greater than 100 μm in length. To increase optical contrast, a probe was sputter-coated with gold-palladium (Hummer 6.2, Anatech); its stiffness was 250 $\mu N \cdot m^{-1}$. A stiff probe was made by pulling a borosilicate capillary to a tip diameter of 1–2 μm. The tip was fire-polished to a diameter of 1 μm and attached to a kinociliary bulb with light suction.

Flexible probes were calibrated by imaging their Brownian motion on the dual photodiode. A Lorentzian fit to the power spectrum of this motion yielded estimates of the probe's

stiffness and drag coefficient (Howard, 2001; Salvi et al., 2015). Probes were displaced by a piezoelectric actuator (PA 4/12, Piezosystem Jena) driven by a 800 mA amplifier (ENV 800, Piezosystem Jena). The actuator was mounted on a micromanipulator (MP-285, Sutter Instruments) to control the fiber's position. The control signal sent to the amplifier was digitally low-pass filtered at 2 kHz.

Signal production and acquisition—All stimuli were controlled with and data were acquired by programs written in LabVIEW (version 16.0; National Instruments). Data were digitized by an analog-to-digital converter and sampled at 50 μs intervals (PCIe-6353, National Instruments). Stimulation and control signals were generated with a digital-to-analog converter (PCI-6733, National Instruments).

Kinociliary dissection—We separated the kinocilium from a hair bundle by first severing the links attaching it to the tallest stereocilia and then forcing it away from the bundle (Hudspeth and Jacobs, 1979). These manipulations were performed with a fine glass pipette pulled with an electrode puller (P-80/PC, Sutter Instruments). The kinociliary links were severed by first sliding the pipette tip between the kinocilium and the tallest stereocilia at a height of 2 μm from the cell surface and then moving the pipette upwards through the kinociliary links.

Ultraviolet and infrared stimulation—We used a 375 nm diode laser (LDM-375, Oxxius) or a 405-nm diode laser (DL-405-100, Crystalaser) to irradiate hair cells with ultraviolet light. Laser beams were focused to the back focal plane of the objective lens to create a collimated beam exiting the objective lens.

We irradiated cells with infrared light from a 1470 nm diode laser (MDL III 1470, Changchun New Industries Optoelectronics Technology Company). The light was delivered with a 105 μm-diameter optical fiber with a flat-cleaved tip (FG105LCA, Thorlabs).

Patterned illumination—We irradiated hair cells with customized illumination patterns by reflecting the light of a 405 nm laser diode (DL-405-100, Crystalaser) from a digital micromirror device (DLP2010, Texas Instruments). Light reflected from micromirrors in the "on" position was collected behind the epifluorescence port of the microscope by a lens (XLFluor 4X, Olympus) to form an image of the surface of the digital micromirror device. This image was relayed and demagnified onto the sample plane through an aspheric lens (ASL-10142-A, Thorlabs) and the objective lens (LumPlanFLN60X, Olympus). Micromirror patterns were loaded on a digital controller (DLPC3435, Texas Instruments) with LabVIEW software (version 16.0, National Instruments).

The micropatterns were visualized by projecting them onto a fluorescein-coated slide and imaging the resulting fluorescence. During an experiment key landmarks such as the boundaries between adjacent rectangles of irradiation were marked on a video screen bearing an image of the sample plane. Each hair cell was then aligned with these landmarks prior to stimulation. In addition, images of the micropattern location and hair cell position were taken in each experiment for post-hoc verification of the positioning.

The responses to stimulation with the digital micromirror device were relatively small owing to our use of a mercury lamp, the luminance of which was lower than that of the lasers. In addition, some light was lost upon reflection from the micromirrors.

Action spectra—Action spectra were elicited with six illumination bands filtered from the emission of a mercury lamp (X-Cite exacte, Excelitas Technologies). The mercury lamp was mounted in the epifluorescence port of the microscope and focused with a lens (AC254-250, ThorLABS) placed 250 mm from the objective lens. Broadband light was filtered and reflected into the sample with six filter and dichroic-mirror sets to give rise to the following wavelength bands (in nanometers): 350–390, 395–415, 426–446, 480–520, 543–557, and 568–590. The filters and dichroic mirrors used in each set were:

FF01-370/36-25, T425lpxr, ET425lp

ET405/20x, T425lpxr, ET430lp

ET436/20x, T470lpxr, ET460lp

ET500/40x, T525lpxr, ET542lp

ET550/15x, T570lpxr, ET570lp

ET580/25x, T605lpxr, ET610lp

All filters and mirrors were obtained from Chroma Technology except the first, which was from Semrock.

To ensure that each wavelength band passed the same intensity of light, the power output in each band was measured using a photodiode-based power meter (S120VC and PM100A, Thorlabs) at all input-command levels of the mercury lamp. The highest power achievable in every band, 5.9 mW, was chosen as the irradiation level. The input command to the mercury lamp was then adjusted to the appropriate value before irradiation with each wavelength band.

Fluorescence imaging—Intracellular chromophores were imaged by epifluorescence excited with a mercury lamp (X-Cite exacte, Excelitas Technologies). NADH was excited at 350–390 nm (FF01-370/36-25, Semrock) and imaged at 425–475 nm (ET450/50m, Chroma). Flavins and hemoproteins were excited at 426–446 nm (ET436/20x, Chroma) and imaged at 510–560 nm (ET550/50m). Images were captured with a CCD camera (ORCA-R2, Hamamatsu).

Temperature measurement—The calibrated resistance of an electrode was used to measure temperature (Yao et al., 2009b). Electrodes were pulled (P-2000, Sutter Instruments) and filled with saline solution identical to that being used in the experiment. Tip resistances ranged from 4–10 MΩ as determined by measuring the current required to elicit a 5 mV voltage drop across the pipette tip with a voltage-clamp amplifier (Axopatch 200B, Molecular Devices). Each electrode was calibrated by recording its resistance at several temperatures. The electrode tip was placed in approximately 2 mL of saline whose temperature was controlled with a chilling and heating dry bath (Echotherm IC20XT, Torrey

Pines). A linear fit to the relation of the logarithm of resistance to the reciprocal of temperature yielded the relation between temperature and resistance.

Heat application by carbon fiber—To rapidly heat cells without irradiating them, we applied local heating pulses with a carbon fiber. Because carbon is an efficient ultraviolet absorber and heat conductor, thermal pulses generated by irradiating a fiber's shank rapidly propagated to its tip. We mounted a single 4.8 μm-diameter carbon fiber (C 005731, Goodfellow) in a pulled glass pipette and positioned its tip 2–5 μm from a hair bundle. The fiber was irradiated approximately 20 μm from its tip with 405 nm light from a laser diode (DL-405-100, Crystalaser). We adjusted the power density of irradiation to elicit the desired temperature increase at the fiber's tip.

Modeling of the thermal pattern around an irradiated hair bundle—For comparison with the measured pattern of temperature changes around a hair bundle, we modeled the steady-state temperature change expected from sources in the mitochondria at the cellular apex. For modest temperature changes, the flow of heat follows the diffusion equation, whose linearity implies that the response at each point in space can be obtained by summing the individual contributions of multiple sources. In an aqueous medium of thermal conductivity $\kappa = 0.60\ \mathrm{W \cdot m^{-1} \cdot K^{-1}}$, the temperature increment ΔT owing to a point source emitting an energy flux f at distance r is

$$\Delta T = \frac{f}{4\pi\kappa r}.$$

We calculated the steady-state temperature change expected for an annular array of 476 point sources, each of 250 nW, surrounding the base of the hair bundle on a 0.25 μm square lattice between radii of 2.5 μm and 4.0 μm (Figure 5B). The offset of approximately 6 °C in the recorded temperatures (Figure 5A) presumably reflects the background of heat production by irradiated mitochondria in the lower portions of the modeled hair cell as well as in the adjacent hair and supporting cells.

Supplementary Material

Refer to Web version on PubMed Central for supplementary material.

Acknowledgments

The authors thank F. Berger, D. Gadsby, A. Kozlov, and R. Rabbitt for helpful discussions, T. Bartsch for assistance with optics, and the members of their research group for critical comments on the manuscript. J.B.A. and N.R.K. were supported by Medical Scientist Training Program grant T32-GM007739 from the National Institutes of Health, and J.B.A. was additionally supported by fellowship F30-DC014215 from the National Institutes of Health. B.A.F. is a Research Technician III and A.J.H. an Investigator of Howard Hughes Medical Institute.

References

Ashmore JF. A fast motile response in guinea-pig outer hair cells: the cellular basis of the cochlear amplifier. J Physiol (Lond). 1987; 388:323–347. DOI: 10.1111/(ISSN)1469-7793 [PubMed: 3656195]

Assad JA, Hacohen N, Corey DP. Voltage dependence of adaptation and active bundle movement in bullfrog saccular hair cells. Proceedings of the National Academy of Sciences. 1989

Azimzadeh JB, Salvi JD. Physiological Preparation of Hair Cells from the Sacculus of the American Bullfrog (Rana catesbeiana). JoVE. 2017; 1:e55380–e55380. DOI: 10.3791/55380

Bayly JG, Kartha VB, Stevens WH. The absorption spectra of liquid phase H_2O, HDO and D_2O from 0.7 μm to 10 μm. Infrared Physics. 1963; 3:211–222. DOI: 10.1016/0020-0891(63)90026-5

Benser ME, Marquis RE, Hudspeth AJ. Rapid, active hair bundle movements in hair cells from the bullfrog's sacculus. J Neurosci. 1996; 16:5629–5643. [PubMed: 8795619]

Berger F, Hudspeth AJ. Chemomechanical regulation of myosin Ic cross-bridges: Deducing the elastic properties of an ensemble from single-molecule mechanisms. PLoS Comput Biol. 2017; 13:e1005566–30. DOI: 10.1371/journal.pcbi.1005566 [PubMed: 28549064]

Berns MW, Gamaleja N, Olson R, Duffy C, Rounds DE. Argon laser micro-irradiation of mitochondria in rat myocardial cells in tissue culture. J Cell Physiol. 1970; 76:207–213. DOI: 10.1002/jcp.1040760211 [PubMed: 5500975]

Liu, Bin, Liu, H., Zhong, D., Lin, C. Searching for a photocycle of the cryptochrome photoreceptors. Current Opinion in Plant Biology. 2010; 13:578–586. DOI: 10.1016/j.pbi.2010.09.005 [PubMed: 20943427]

Bozovic D, Hudspeth AJ. Hair-bundle movements elicited by transepithelial electrical stimulation of hair cells in the sacculus of the bullfrog. Proc Natl Acad Sci USA. 2003; 100:958–963. DOI: 10.1073/pnas.0337433100 [PubMed: 12538849]

Brownell WE, Bader CR, Bertrand D, de Ribaupierre Y. Evoked mechanical responses of isolated cochlear outer hair cells. Science. 1985; 227:194–196. [PubMed: 3966153]

Butt WD, Keilin D. Absorption spectra and some other properties of cytochrome c and of its compounds with ligands. Proc R Soc Lond, B, Biol Sci. 1962; 156:429–458. [PubMed: 14040866]

Cheung ELM, Corey DP. Ca2+ changes the force sensitivity of the hair-cell transduction channel. Biophysj. 2006; 90:124–139. DOI: 10.1529/biophysj.105.061226

Choe Y, Magnasco MO, Hudspeth AJ. A model for amplification of hair-bundle motion by cyclical binding of Ca2+ to mechanoelectrical-transduction channels. Proc Natl Acad Sci USA. 1998; 95:15321–15326. [PubMed: 9860967]

Corey, DP. Dissertation thesis. 1980. A biophysical approach to sensory transduction by vertebrate hair cells.

Corns LF, Johnson SL, Kros CJ, Marcotti W. Calcium entry into stereocilia drives adaptation of the mechanoelectrical transducer current of mammalian cochlear hair cells. Proc Natl Acad Sci USA. 2014; doi: 10.1073/pnas.1409920111

Dittami GM, Rajguru SM, Lasher RA, Hitchcock RW, Rabbitt RD. Intracellular calcium transients evoked by pulsed infrared radiation in neonatal cardiomyocytes. J Physiol (Lond). 2011; 589:1295–1306. DOI: 10.1113/jphysiol.2010.198804 [PubMed: 21242257]

Ellis-Davies GC, Kaplan JH. Nitrophenyl-EGTA, a photolabile chelator that selectively binds Ca2+ with high affinity and releases it rapidly upon photolysis. Proc Natl Acad Sci USA. 1994; 91:187–191. [PubMed: 8278362]

Goyal V, Rajguru S, Matic AI, Stock SR, Richter CP. Acute Damage Threshold for Infrared Neural Stimulation of the Cochlea: Functional and Histological Evaluation. Anat Rec. 2012; 295:1987–1999. DOI: 10.1002/ar.22583

Gupte SS, Hackenbrock CR. The role of cytochrome c diffusion in mitochondrial electron transport. J Biol Chem. 1988; 263:5248–5253. [PubMed: 2833502]

Hernandez VH, Gehrt A, Reuter K, Jing Z, Jeschke M, Mendoza Schulz A, Hoch G, Bartels M, Vogt G, Garnham CW, Yawo H, Fukazawa Y, Augustine GJ, Bamberg E, Kügler S, Salditt T, de Hoz L, Strenzke N, Moser T. Optogenetic stimulation of the auditory pathway. J Clin Invest. 2014; 124:1114–1129. DOI: 10.1172/JCI69050 [PubMed: 24509078]

Howard, J. Mechanics of Motor Proteins and the Cytoskeleton. Sunderland, MA: Sinauer; 2001.

Howard J, Hudspeth AJ. Compliance of the hair bundle associated with gating of mechanoelectrical transduction channels in the bullfrog's saccular hair cell. Neuron. 1988; 1:189–199. [PubMed: 2483095]

Howard J, Hudspeth AJ. Mechanical relaxation of the hair bundle mediates adaptation in mechanoelectrical transduction by the bullfrog's saccular hair cell. Proc Natl Acad Sci USA. 1987; 84:3064–3068. [PubMed: 3495007]

Howard J, Spudich JA. Is the lever arm of myosin a molecular elastic element? Proc. Natl Acad Sci USA. 1996; 93:4462–4464.

Hudspeth AJ. Integrating the active process of hair cells with cochlear function. Nat Rev Neurosci. 2014; doi: 10.1038/nrn3786

Hudspeth AJ. Making an effort to listen: mechanical amplification in the ear. Neuron. 2008; 59:530–545. DOI: 10.1016/j.neuron.2008.07.012 [PubMed: 18760690]

Hudspeth, AJ. Hair-bundle mechanics and a model for mechanoelectrical transduction by hair cells. In: Corey, DP., Roper, SD., editors. Sensory Transduction Society of General Physiologists Th Annual Symposium. 1992. p. 357-370.

Hudspeth AJ, Corey DP. Controlled bending of high-resistance glass microelectrodes. Am J Physiol. 1978; 234:C56–7. [PubMed: 623241]

Hudspeth AJ, Jacobs R. Stereocilia mediate transduction in vertebrate hair cells (auditory system/cilium/vestibular system). Proc Natl Acad Sci USA. 1979; 76:1506–1509. [PubMed: 312502]

Kallweit N, Baumhoff P, Krueger A, Tinne N, Kral A, Ripken T, Maier H. Optoacoustic effect is responsible for laser-induced cochlear responses. Sci Rep. 2016; 6:1–10. DOI: 10.1038/srep28141 [PubMed: 28442746]

Kennedy HJ, Crawford AC, Fettiplace R. Force generation by mammalian hair bundles supports a role in cochlear amplification. Nature. 2005; 433:880–883. DOI: 10.1038/nature03367 [PubMed: 15696193]

Kozlov AS, Risler T, Hudspeth AJ. Coherent motion of stereocilia assures the concerted gating of hair-cell transduction channels. Nat Neurosci. 2007; 10:87–92. DOI: 10.1038/nn1818 [PubMed: 17173047]

Liu Q, Frerck MJ, Holman HA, Jorgensen EM, Rabbitt RD. Exciting Cell Membranes with a Blustering Heat Shock. Biophysj. 2014; 106:1570–1577. DOI: 10.1016/j.bpj.2014.03.008

Lumbreras V, Bas E, Gupta C, Rajguru SM. Pulsed infrared radiation excites cultured neonatal spiral and vestibular ganglion neurons by modulating mitochondrial calcium cycling. Journal of Neurophysiology. 2014; 112:1246–1255. DOI: 10.1152/jn.00253.2014 [PubMed: 24920028]

Martin P, Hudspeth AJ. Active hair-bundle movements can amplify a hair cell's response to oscillatory mechanical stimuli. Proc Natl Acad Sci USA. 1999; 96:14306–14311. [PubMed: 10588701]

Paltauf G, Schmidt-Kloiber H, Frenz M. Photoacoustic waves excited in liquids by fiber-transmitted laser pulses. J Acoust Soc Am. 1998; 104:890–897. DOI: 10.1121/1.423334

Peng AW, Effertz T, Ricci AJ. Adaptation of Mammalian auditory hair cell mechanotransduction is independent of calcium entry. Neuron. 2013; 80:960–972. DOI: 10.1016/j.neuron.2013.08.025 [PubMed: 24267652]

Rabbitt RD, Brichta AM, Tabatabaee H, Boutros PJ, Ahn J, Santina, Della CC, Poppi LA, Lim R. Heat pulse excitability of vestibular hair cells and afferent neurons. Journal of Neurophysiology. 2016; 116:825–843. DOI: 10.1152/jn.00110.2016 [PubMed: 27226448]

Rajguru SM, Richter CP, Matic AI, Holstein GR, Highstein SM, Dittami GM, Rabbitt RD. Infrared photostimulation of the crista ampullaris. J Physiol (Lond). 2011; 589:1283–1294. DOI: 10.1113/jphysiol.2010.198333 [PubMed: 21242259]

Richardson RT, Thompson AC, Wise AK, Needham K, Richardson RT, Thompson AC, Wise AK, Needham K. Challenges for the application of optical stimulation in the cochlea for the study and treatment of hearing loss. Expert Opinion on Biological Therapy. 2017; 17:213–223. DOI: 10.1080/14712598.2017.1271870 [PubMed: 27960585]

Richter, C-P., Rajguru, S., Bendett, M. Infrared neural stimulation in the cochlea. In: Kollias, N.Choi, B.Zeng, H.Kang, HW.Knudsen, BE.Wong, BJ.Ilgner, JF.Suter, MJ.Lam, S.Brenner, M.Gregory, KW.Tearney, GJ.Marcu, L.Hirschberg, H.Madsen, SJ.Mahadevan-Jansen, A.Jansen, ED.Mandelis, A., Morris, MD., editors. Presented at the SPIE BiOS; SPIE; 2013. p. 85651Y-10.

Rosin C, Erlkamp M, Ecken, von der J, Raunser S, Winter R. Exploring the Stability Limits of Actin and Its Suprastructures. Biophysj. 2014; 107:2982–2992. DOI: 10.1016/j.bpj.2014.11.006

Salet C. A study of beating frequency of a single myocardial cell. I. Q-switched laser microirradiation of mitochondria. Exp Cell Res. 1972; 73:360–366. [PubMed: 4115483]

Salvi JD, Ó Maoiléidigh D, Fabella BA, Tobin M, Hudspeth AJ. Control of a hair bundle's mechanosensory function by its mechanical load. Proc Natl Acad Sci USA. 2015; 112:E1000–9. DOI: 10.1073/pnas.1501453112 [PubMed: 25691749]

Shapiro MG, Homma K, Villarreal S, Richter CP, Bezanilla F. Infrared light excites cells by changing their electrical capacitance. Nature Communications. 2012; 3:376–10. DOI: 10.1038/ncomms1742

Siegel JM, Montgomery GA, Bock RM. Ultraviolet absorption spectra of DPN and analogs of DPN. Arch Biochem Biophys. 1959; 82:288–299. [PubMed: 13661953]

Teudt IU, Maier H, Richter C-P, Kral A. Acoustic Events and "Optophonic" Cochlear Responses Induced by Pulsed Near-Infrared LASER. IEEE Trans Biomed Eng. 2011; 58:1648–1655. DOI: 10.1109/TBME.2011.2108297 [PubMed: 21278011]

Thompson AC, Fallon JB, Wise AK, Wade SA, Shepherd RK, Stoddart PR. Infrared neural stimulation fails to evoke neural activity in the deaf guinea pig cochlea. Hearing Research. 2015; 324:46–53. DOI: 10.1016/j.heares.2015.03.005 [PubMed: 25796297]

Tinevez JY, Jülicher F, Martin P. Unifying the various incarnations of active hair-bundle motility by the vertebrate hair cell. Biophysical Journal. 2007; 93:4053–4067. DOI: 10.1529/biophysj.107.108498 [PubMed: 17704173]

Verma RU, Guex AA, Hancock KE, Durakovic N, McKay CM, Slama MCC, Brown MC, Lee DJ. Auditory responses to electric and infrared neural stimulation of the rat cochlear nucleus. Hearing Research. 2014; 310:69–75. DOI: 10.1016/j.heares.2014.01.008 [PubMed: 24508368]

Wells J, Kao C, Mariappan K, Albea J, Jansen ED, Konrad P, Mahadevan-Jansen A. Optical stimulation of neural tissue in vivo. Opt Lett OL. 2005; 30:504–506. DOI: 10.1364/OL.30.000504

Wu YC, Ricci AJ, Fettiplace R. Two components of transducer adaptation in auditory hair cells. Journal of Neurophysiology. 1999; 82:2171–2181. [PubMed: 10561397]

Yao J, Liu B, Qin F. Rapid Temperature Jump by Infrared Diode Laser Irradiation for Patch-Clamp Studies. Biophysj. 2009a; 96:3611–3619. DOI: 10.1016/j.bpj.2009.02.016

Yao J, Liu B, Qin F. Rapid temperature jump by infrared diode laser irradiation for patch-clamp studies. Biophysical Journal. 2009b; 96:3611–3619. DOI: 10.1016/j.bpj.2009.02.016 [PubMed: 19413966]

HIGHLIGHTS

- Hair cells respond mechanically and electrically to ultraviolet light.
- These responses involve the opening of mechanotransduction channels.
- Temperature measurements demonstrate that the responses stem from local heating.
- Heat both softens gating springs and opens mechanotransduction channels.

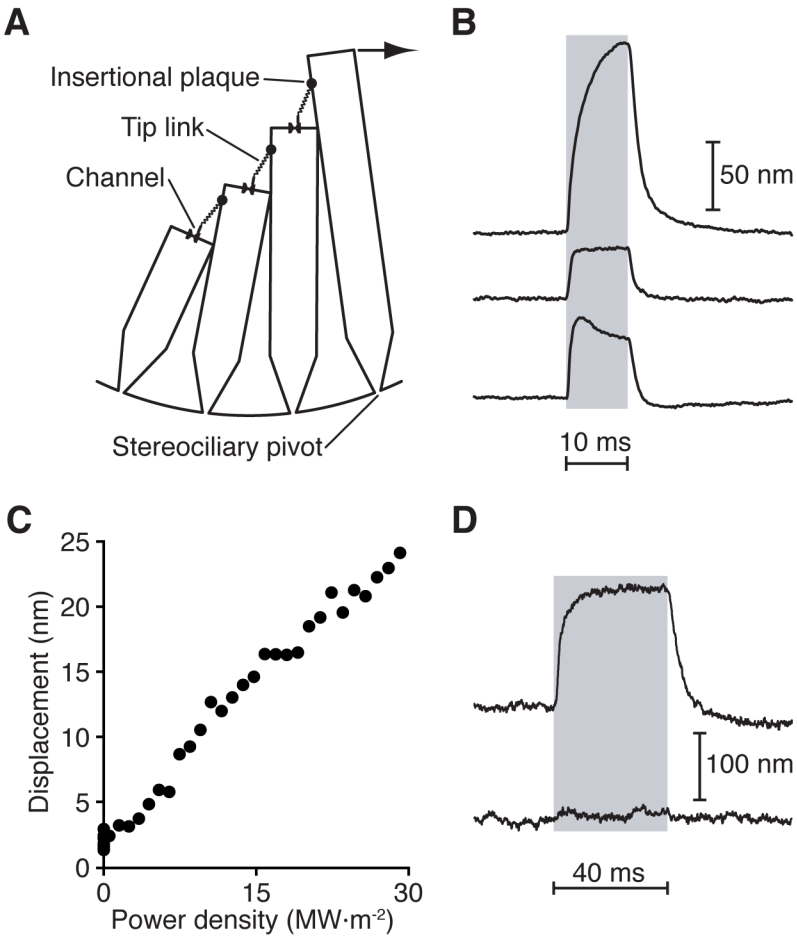

Figure 1. Light-evoked hair-bundle movement

(A) A schematic drawing of a hair bundle depicts a file of four actin-filled stereocilia; the kinocilium is not shown. At the tip of each stereocilium a single tip link inserts upon one or two mechanically sensitive ion channels. Application of a force (arrow) in the positive direction, toward the bundle's tall edge, tenses the tip links and opens the channels. At the insertional plaque atop each tip link, myosin motors adjust the tension in the link and thus regulate the probability of channel opening. (B) Irradiation with ultraviolet light of three different hair cells from the bullfrog's sacculus evoked hair-bundle movements with distinct timecourses. To record hair-bundle motion, the shadow of a hair bundle was projected onto a dual photodiode (see Methods). In this and subsequent figures, a gray or purple band denotes the duration of irradiation. Wavelength, 375 nm; power density, 152 $MW \cdot m^{-2}$ (1 $MW \cdot m^{-2}$ = 1 $W \cdot mm^{-2}$). (C) The peak amplitude of hair-bundle movement increased linearly with the power density of illumination. (D) Measurements of light-induced hair-bundle motion before (upper trace) and after (lower trace) iontophoretic application of EGTA demonstrated that the response required intact tip links. Data were obtained from hair bundles embedded in the saccular macula and irradiated from a direction orthogonal to the plane of the macula. See also Figures S1 and S2 and Movies S1 and S2.

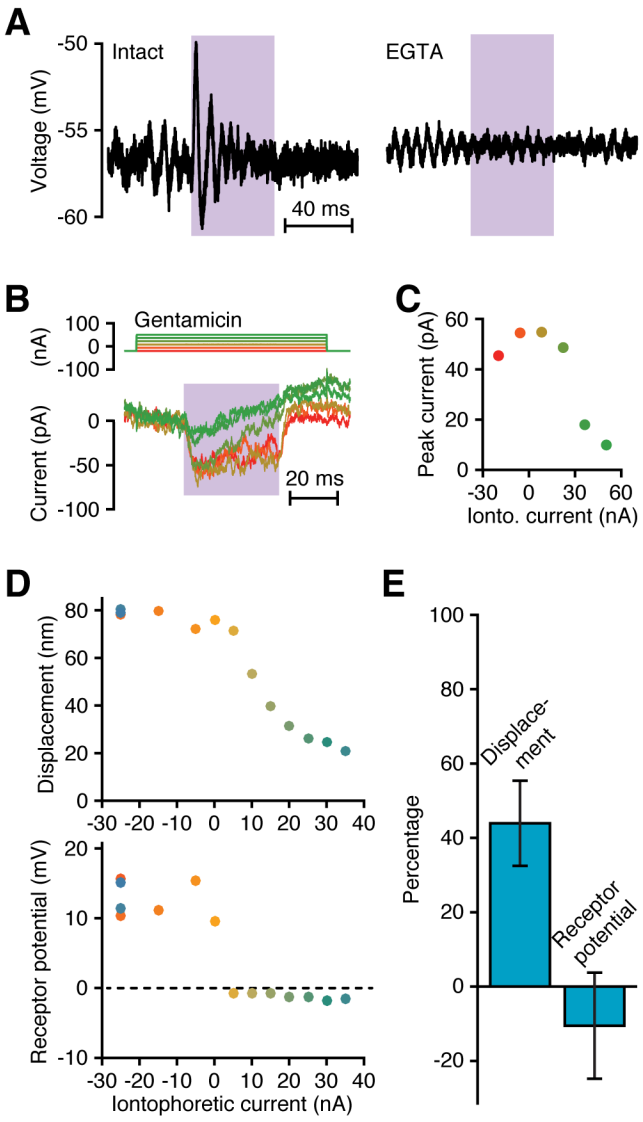

Figure 2. Light-evoked activation of mechanotransduction channels

(A) Microelectrode recordings of receptor potentials recorded from hair cells before (left) and after (right) treatment with EGTA demonstrated that intact tip links were required for the light-evoked response. The light-induced depolarization triggered oscillation of the membrane potential owing to the cell's electrical-tuning mechanism; some noise-induced oscillation also occurred in both records. In the intact hair cell, the peak-to-trough response to the laser was 8.8 mV and the RMS noise was 1.5 mV. For the disrupted hair cell, the peak-to-trough value during irradiation was 0.8 mV and the RMS noise was 0.9 mV. Wavelength, 375 nm; power density, 106 $MW \cdot m^{-2}$. (B) Tight-seal, whole-cell recordings (lower traces) show that the light-evoked inward current diminished with increasing iontophoresis of the channel blocker gentamicin (upper traces). (C) The average peak laser-evoked current, recorded 3–9 ms after the onset of irradiation, declined with increasing iontophoretic current, demonstrating that irradiation opened mechanotransduction channels. Wavelength, 375 nm; power density, 106 $MW \cdot m^{-2}$. (D) Simultaneous measurements of hair-

bundle displacements and receptor potentials recorded with sharp microelectrodes show that the receptor potential was eliminated at the highest gentamicin concentrations, but some bundle motion persisted. Data were collected in the order shown by a chromatic scale running from red to dark blue. Note that repetition of the control points at the strongest holding current yielded results consistent with those at the experiment's outset. Resting potential, −52 mV; wavelength, 375 nm; power density, 106 $MW \cdot m^{-2}$. (E) A histogram displays the mean responses with standard deviations of four hair cells to iontophoretic expulsion of gentamicin at currents of +35 nA to +70 nA as a percentage of the control levels for holding currents of −30 nA to −10 nA. Although the drug completely abolishes the receptor potential, it consistently spares a substantial percentage of the mechanical response. The cells in panels A, D, and E remained in the saccular epithelium and were irradiated from a direction orthogonal to the plane of the sacculus. The cell in panel B and C was extruded from the epithelium and was illuminated from a direction orthogonal to the hair bundle's axis of sensitivity. See also Figure S3.

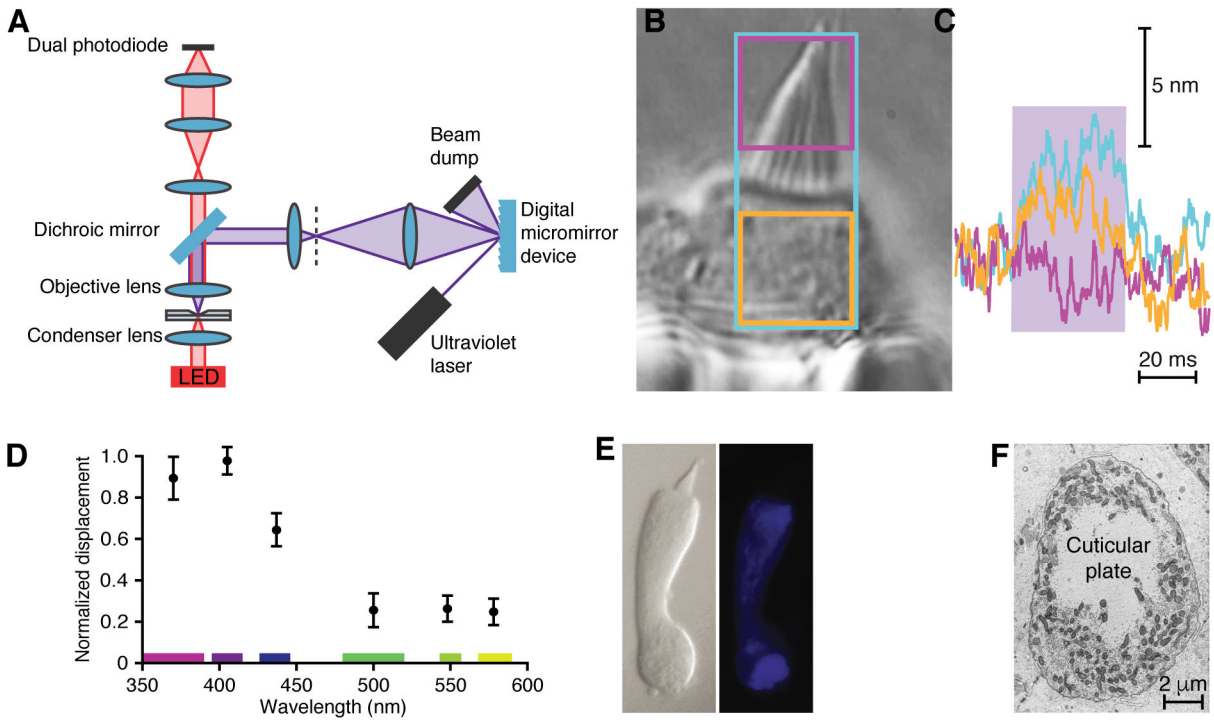

Figure 3. Localization and action spectrum of intracellular absorbers

(A) A schematic diagram portrays the optical pathway by means of which a digital micromirror device projected light patterns onto specific parts of an isolated hair cell. (B) The cell was held in a polished glass pipette with the apical end of the soma and the hair bundle protruding. The three colored rectangles outline the areas irradiated for the correspondingly colored records in the following panel. (C) Hair-bundle displacement was maximal when the largest area was illuminated (blue trace; blue rectangle in panel b). Irradiation of the hair bundle alone did not evoke motion (magenta trace; magenta rectangle in panel b). Irradiation of the area immediately below the hair bundle elicited nearly maximal motion (orange trace; orange rectangle in B), indicating that this region contained most of the light absorbers responsible for the response. Power densities: blue trace, 4.8 $MW \cdot m^{-2}$; magenta trace, 4.3 $MW \cdot m^{-2}$; orange trace, 4.4 $MW \cdot m^{-2}$. (D) The action spectrum of light-evoked hair-bundle motion shows a maximal response in the 400 nm wavelength band. The means and standard deviations for 11 cells are plotted. The width of each wavelength band is indicated in the corresponding color along the abscissa. The average deflection in the 400 nm band was 35.2 nm, whereas the RMS noise was 1.9 nm. (E) Left: A differential-interference-contrast image shows a dissociated hair cell. Middle: Ultraviolet illumination revealed the autofluorescence of intracellular NADH in the same cell. Right: Blue-light excitation evoked the autofluorescence of cytochromes and oxidized flavins in the identical cell. (F) A transmission electron micrograph depicts a plane of section parallel with the apical surface of the saccular sensory epithelium. Densely packed mitochondria surround the cuticular plate at the apex of a hair cell's soma.

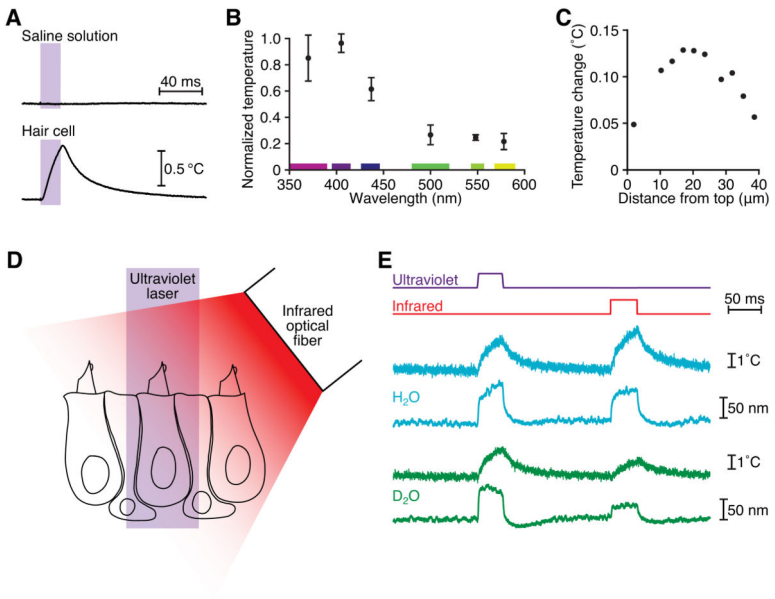

Figure 4. Thermal stimulation of hair cells

(A) Ultraviolet irradiation of a hair cell led to heat generation, whereas irradiation of saline solution did not. This cell remained in the saccular epithelium and was irradiated from a direction orthogonal to the plane of the sacculus. The calibrated resistance of a microelectrode was used to record the temperature. (B) A temperature action spectrum reveals that heat production peaked in the 400 nm wavelength band. The means and standard deviations for four cells are plotted. The cells remained in the epithelium and were irradiated from a direction orthogonal to the plane of the sacculus. (C) Temperature measurements along a transect 2 μm from the lateral edge of a dissociated hair cell revealed that the largest temperature increases occurred basal to the hair bundle, whose top is situated at 0 μm and whose bottom is indicated by the dotted vertical line. This result accords with intra-mitochondrial light absorbers as the source of heat. (D) A schematic drawing depicts a hair bundle positioned beneath one beam of ultraviolet light and another of infrared light so that the bundle could be stimulated at either wavelength. (E) A hair bundle in H_2O-based saline solution exhibited similar movements and local temperature increases (blue) for ultraviolet illumination at a power density of 71 $MW \cdot m^{-2}$ and for infrared irradiation at a power density of 0.13 $MW \cdot m^{-2}$. After substitution of D_2O-based saline solution, the same hair bundle showed similar decreases in displacement and temperature change during infrared but not ultraviolet illumination (green). Temperature records were taken 2 μm from the side of the bundle, at a height of 7 μm above the apical epithelial surface.

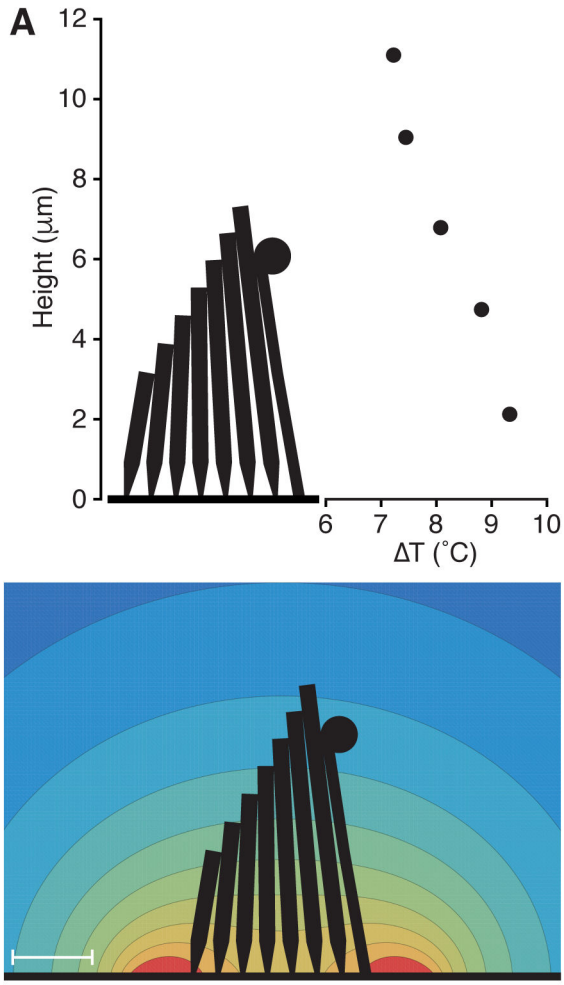

Figure 5. Localization of the heat source underlying hair-bundle movement

(A) While a hair cell in the saccular epithelium was irradiated from above with ultraviolet light, we measured the temperature increase (ΔT) along a trajectory 2 μm from the kinocilium and at various heights above the epithelial surface. The silhouette of a hair bundle is drawn to scale for reference. Wavelength, 405 nm; power density, 50 $MW \cdot m^{-2}$. (B) The steady-state temperature changes expected from the heat equation were derived for an array of point sources surrounding the hair bundle. Isotemperature contours are shown at intervals of 0.5 °C from 5.5 °C to 1.5 °C. The calculated profile is consistent with the spatial pattern recorded above the hair cell. See also Figure S5.

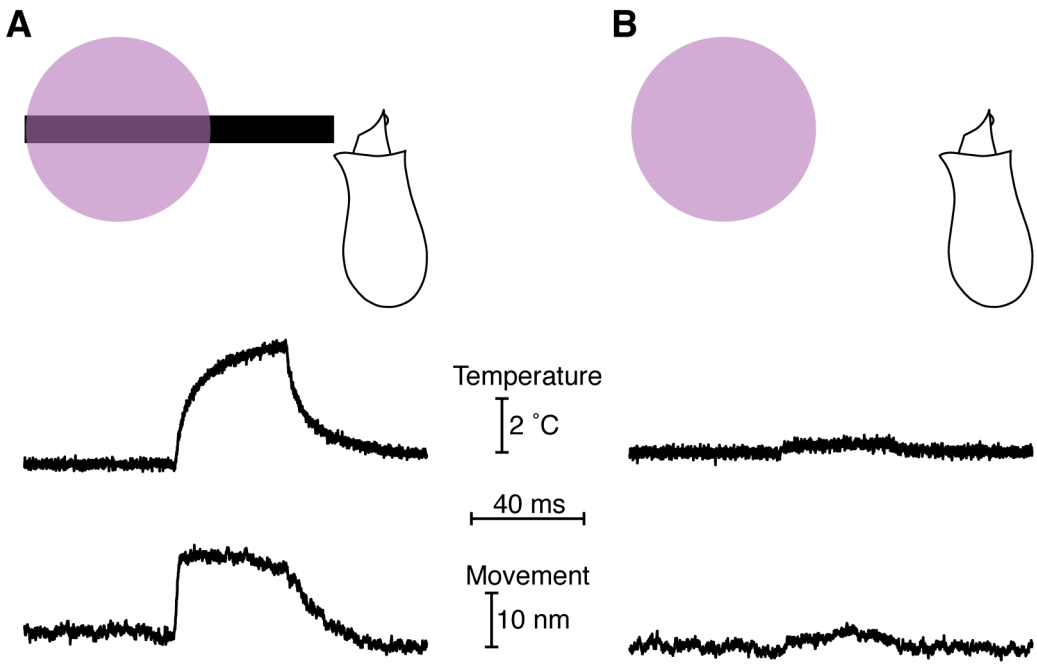

Figure 6. Hair-bundle movement elicited by heat pulses

(A) A 5 μm-diameter carbon fiber was positioned beneath a laser beam with its tip extending beyond the beam to a position 3 μm from the hair bundle of a dissociated hair cell. The temperature was measured with a calibrated electrode 2 μm beyond the kinociliary bulb. When illuminated, the carbon fiber radiated heat and caused hair-bundle motion. (B) Upon retraction of the carbon fiber, both the ultraviolet light-evoked temperature increase and the hair-bundle motion were reduced, confirming that the temperature change was responsible for hair-bundle motion. Wavelength, 405 nm; power density, 50 $MW \cdot m^{-2}$.

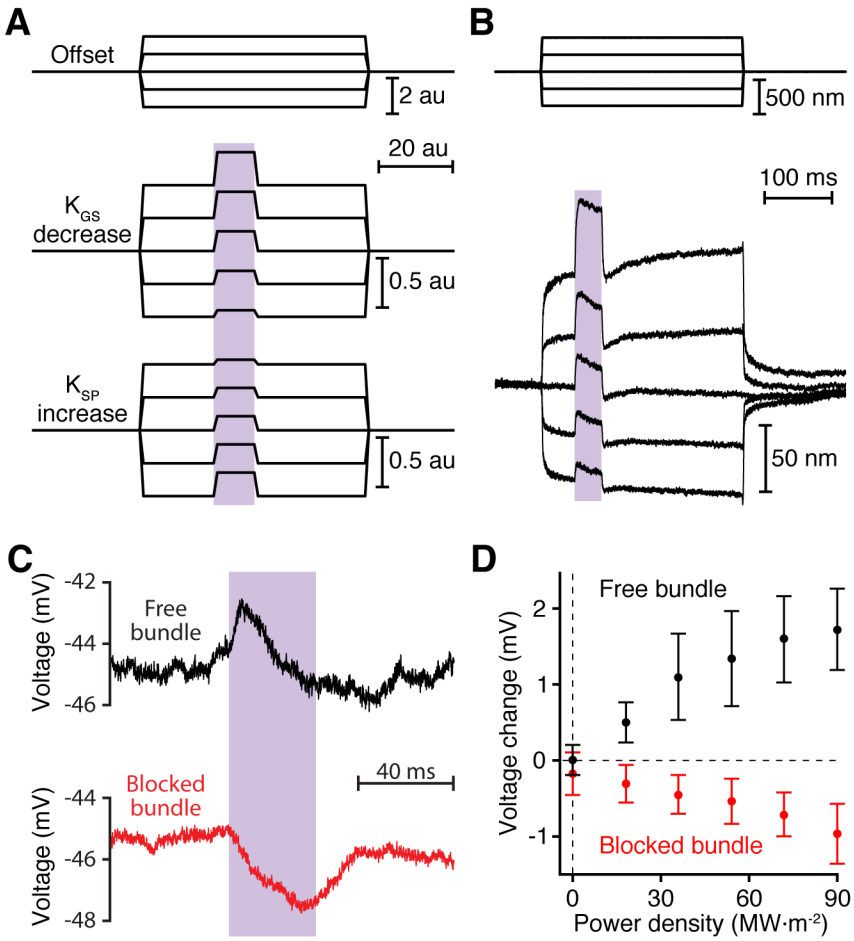

Figure 7. Effect of heating the gating springs

(A) A hair bundle can be modeled as a pair of opposing elastic elements: the gating springs that tug the bundle in the negative direction and the stereociliary pivots that pull in the opposite direction. When a hair bundle undergoes a positive movement in response to illumination, the distinct effects of offsets imposed by a flexible fiber of stiffness K_{FIBER} (upper traces) distinguish a decrease in the stiffness of the gating springs (K_{GS}, middle traces) from an increase in the stiffness of the stereociliary pivots (K_{SP}, lower traces). Arbitrary parameter values: K_{GS} = 100; X_{GS} = −1; K_{SP} = 100; X_{SP} = 1; K_{FIBER} = 100; fiber-base offset commands = −2, −1, 0, 1, 2; au = arbitrary unit. To model a reduction in gating-spring stiffness during the laser pulse, we diminished K_{GS} by 50 %; to represent an increase in stereociliary-pivot stiffness, we augmented K_{SP} by 50 %. (B) While exposed to iontophoretically applied gentamicin to block transduction, an actual hair bundle of a hair cell in the saccular epithelium was offset with a flexible glass fiber (upper traces). Fifty milliseconds after the initiation of the offset, the bundle was irradiated with ultraviolet light for 40 ms. The resultant hair-bundle motion (lower traces) accorded with the expectation for a heat-induced decrease in gating-spring stiffness. Iontophoretic current, 70 nA; fiber stiffness, 280 $\mu N \cdot m^{-1}$; wavelength, 405 nm; power density, 83 $MW \cdot m^{-2}$. (C) A pulse of ultraviolet light depolarized a hair cell in the saccular epithelium whose hair bundle was free to move (black). When the same bundle was prevented by a stiff glass fiber from moving

towards its kinocilium, identical irradiation instead produced hyperpolarization (red). (D) The peak responses to various levels of illumination, taken as the mean membrane potentials in a 2–7 ms window around the peaks less the baseline values, are plotted against the power densities of irradiation. The error bars represent the standard deviations of responses from six hair cells. See also Figure S6.